

Search for Axions and Dark Photons Using Single Molecule Magnets

Jose R. Alves^{1,2,3}, Manfred Lindner³, Farinaldo S. Queiroz^{1,2,4,5}, Manoel S. Vasconcelos^{1,6}

¹Departamento de Física, Universidade Federal do Rio Grande do Norte, 59078-970, Natal, RN, Brasil

²International Institute of Physics, Universidade Federal do Rio Grande do Norte,

Campus Universitário, Lagoa Nova, Natal-RN 59078-970, Brazil

³Max Planck Institut für Kernphysik, Heidelberg, Germany

⁴Millennium Institute for Subatomic Physics at the High-Energy

Frontier (SAPHIR) of ANID, Fernandez Concha 700, Santiago, Chile

⁵Departamento de Física, Facultad de Ciencias,

Universidad de La Serena, Avenida Cisternas 1200, La Serena, Chile

⁶Programa de Pós Graduação em Física, Universidade do Estado do Rio Grande do Norte, Mossoró-RN, 59610-210, Brasil

(Dated: January 6, 2026)

Molecular magnets, although analogous to familiar macroscopic magnets, offer a platform for next generation magnetic storage technologies with far higher data densities and prospective applications in quantum information science. When exposed to an external magnetic field, single molecule magnets enter a frustrated magnetic configuration that is exceptionally sensitive to low energy excitations. Energy deposited by a dark matter particle can trigger the relaxation of a metastable molecule, releasing Zeeman energy that subsequently propagates through neighboring molecules. This magnetic avalanche encodes the energy deposited in the initial excitation. By combining concepts from chemistry, condensed matter physics, and particle physics, we show that dysprosium and manganese molecules can achieve more than an order of magnitude improvement in sensitivity to dark photon and QCD axion models, respectively, compared with existing detection methods.

INTRODUCTION

The existence of non-baryonic dark matter (DM), a dominant component shaping galactic structures and galaxy clusters, is firmly established through extensive cosmological and astrophysical evidence [1]. Yet its fundamental nature remains elusive. The two leading interpretations—primordial black holes [2] and elementary particles—present distinct pathways; here we focus on the latter. This approach necessitates non-negligible interactions between DM and Standard Model (SM) particles to enable experimental detection.

Searches for DM via nuclear scattering [3–5], astrophysical signatures [6, 7], and accelerator production [8, 9] have excluded many minimal weakly interacting DM models. Future experiments like LUX-ZEPLIN [10], XENONnT, and PandaX-4T may soon achieve detection. However, for sub-GeV DM masses, nuclear recoils are suppressed. A DM particle with mass M will carry energy $E = 1/2Mv^2 \sim 10^{-6}M$, yielding recoils below the keV thresholds of conventional detectors. While electron-recoil experiments extend sensitivity to MeV masses [11, 12], lighter DM remains inaccessible—motivating our novel approach.

Notably, dark matter particles in the Milky Way halo may undergo acceleration through elastic collisions with high-energy galactic cosmic rays and astrophysical neutrinos [13–18]. This inevitable “boosted dark matter” (BDM) component, though small, carries sufficient kinetic energy to be constrained by direct detection experiments. However, when the mediator of the DM-target interaction is light, ($M_{med} \ll q$), sensitivity degrades due to momentum-dependent form factors. While existing

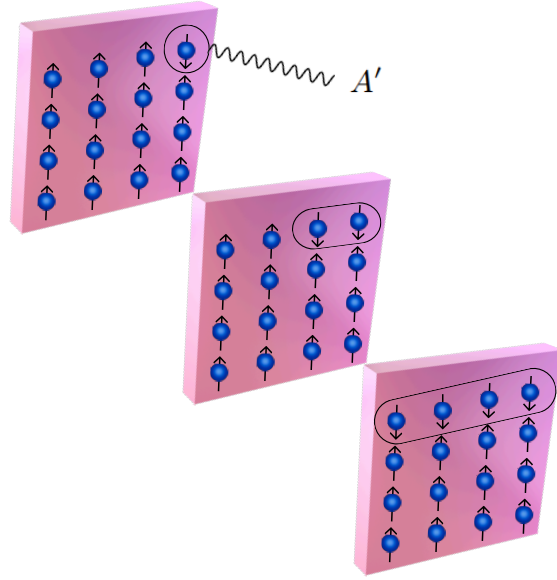


FIG. 1: Sketch of the detection mechanism proposed in the paper. From left to right: the DM particle hits one of the molecules in the metastable state, which relaxes, releasing the Zeeman energy stored, which then propagates to the neighboring molecules, as shown by the red dashed circle increasing in size, in a process known as magnetic avalanche.

BDM studies focus primarily on keV-scale masses, we target the unexplored sub-eV regime, where conventional detectors lack sensitivity.

Motivated by this gap, we leverage condensed-matter systems—building on proposals using semiconductors

[19, 20], photonic nanostructures [21], Fermi-degenerate materials [22], and magnetic bubbles [23]. Specifically, we propose dysprosium-based single-molecule magnets (SMMs) as BDM detectors: the dinuclear complex Dy_2 , and the complex Dy^{III} (illustrated in FIGS.2-3) both exhibiting robust SMM behavior [24, 25]. We further incorporate far-infrared spectra of Manganese, Mn_{12} -acetate [26, 27] to probe *axion* masses across complementary frequency bands.

These systems maintain metastable magnetic states (See. FIGS.4a-4b) for extended periods at cryogenic temperatures $T \sim 0.1$ K. They have attracted considerable interest due to their applications in magnetic storage and potential use as qubits in quantum computing [28]. This characteristic of staying in a false vacuum with a relatively long period allows us to probe dark sectors via the absorption of a BDM as illustrated in FIG.1.

We derive the physics reach of this new method for two popular dark matter models: *dark photon* and *axion*. The *dark photon* arises as the gauge boson of an extended $U(1)'$ symmetry in the SM Lagrangian via the interaction term, [29],

$$\mathcal{L}_{DP} \supset -\frac{\epsilon}{2} F_{\mu\nu} F'^{\mu\nu}, \quad (1)$$

where ϵ is the kinetic mixing. The *axion* particle has been introduced to solve the strong CP problem as a result of the Peccei–Quinn symmetry [30–32]. In the end, this solution induces a coupling to the electromagnetic field strength tensor described by [33, 34],

$$\mathcal{L}_a \supset -\frac{1}{4} g_{a\gamma\gamma} a F_{\mu\nu} \tilde{F}^{\mu\nu}. \quad (2)$$

Because this work spans several disciplines, we begin by introducing the essential concepts of SSMs and molecular absorption. We then show that, for particle masses below 1 eV, these systems provide a uniquely powerful platform where particle physics, condensed matter physics, and chemistry intersect, enabling a detection strategy with the potential to surpass the sensitivity of existing experimental approaches by more than one order of magnitude.

SINGLE MOLECULE MAGNETS

In this section, we outline the key properties of SSMs that underpin their use as dark-matter sensors and review the essential principles governing absorption in SSMs to establish how the ensuing magnetic avalanche encodes the energy deposited by an incident DM particle.

SSMs exhibit magnetic properties similar to those of bulk magnetic material. The term *single-molecule* magnet means that the considered molecule is a magnet itself, with a unique domain. In bulk magnets, the magnetic

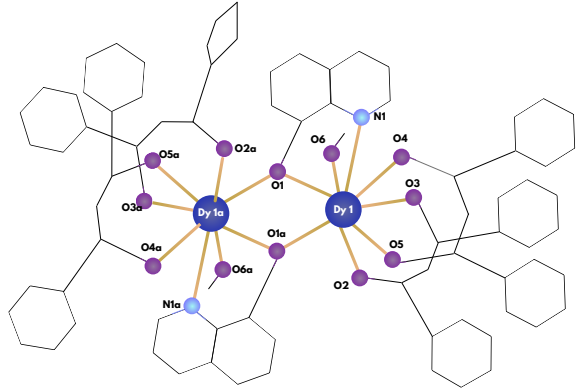


FIG. 2: It illustrates the dinuclear dysprosium. The dark blue spheres represent the dysprosium nuclei, the purple circles the oxygen atoms, and the light blue spheres the nitrogen.

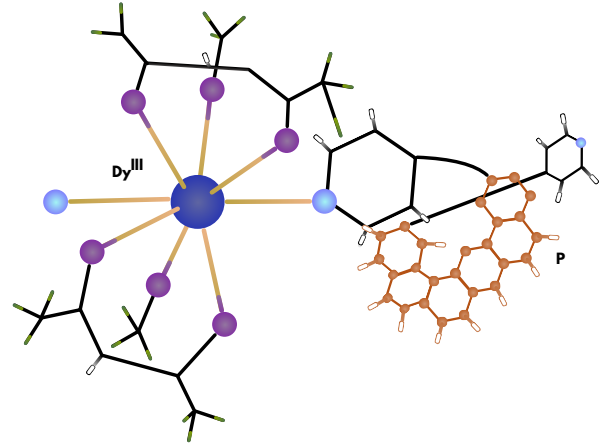
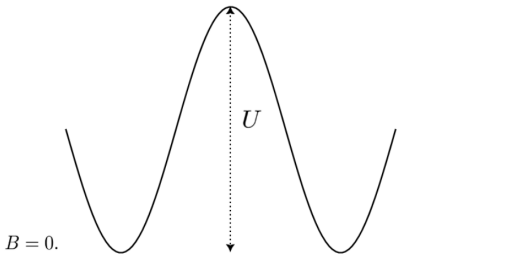


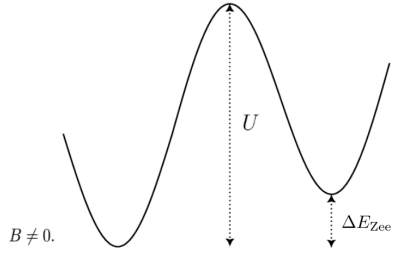
FIG. 3: Figure displaying Dy^{III} . The dysprosium atom is in dark blue, oxygen in purple, and nitrogen in light blue. Highlighted in orange is the helical helicity center for the compound, which drives the compound's chiral features.

moment arises from the presence of unpaired electrons, meaning their spins form parallel/antiparallel arrangements within domains (this is what we call the areas separated by Bloch domain walls). As well as in bulk materials, the SMMs can be magnetized by an external magnetic field, and are demagnetized when this external magnetic field is removed. We work with lanthanides, which are a class of f-block metals, in order to describe its magnetic properties, we need to consider spin-orbit coupling terms, characterized by the quantum number J , i.e., the total angular momentum, and their splitting by the applied field, leading to sublevels that are described by E_J instead of quantum numbers E_S [35].

It has been found that its magnetization slowly relaxes with the removal of an applied external magnetic field, and the relaxation timescale is different from that of bulk



(a) Splitting of the potential felt by an SMM without an external magnetic field.



(b) Splitting of the potential felt by an SMM with an external magnetic field.

FIG. 4: The potential felt by an SMM molecule, FIG.4a shows the potential without an external magnetic field, picturing the degenerate vacuum, while FIG.4b pictures one of the vacuum lifted due to the presence of an external magnetic field. The mechanism proposed focuses on the latter.

materials; however, some molecules can have their relaxation timescale made large enough for the proposed experiment for low temperatures, as in Eq. (4). The relaxation time for this process will be discussed below. Therefore, these new molecules have induced a new concept in the field of magnets, generating interesting experimental and theoretical consequences, such as out-of-phase signals in AC studies of magnetic properties [36]. Most of these molecules exhibit a large effective spin ground state S that may appear due to exchange of ions in the magnetic core (as is the case for Mn12-acetate, whose S is equal to 10 [35, 37]) or competing antiferromagnetic interaction between the spins of the ions, alongside an axial zero-field splitting which separates the $(2S+1)$ m_s projections of the spin in the z -axis (or easy axis of the molecule). This splitting is characterized by a parameter D present in the Hamiltonian that describes these molecules, which is given by,

$$H \supset -DS_z^2. \quad (3)$$

This Hamiltonian nicely describes the system at low temperatures. For $D > 0$ the low-lying energy levels are those with the highest $|E_S|$ value, in this case $E_S = \pm S$. The magnetization of the molecule is associated with

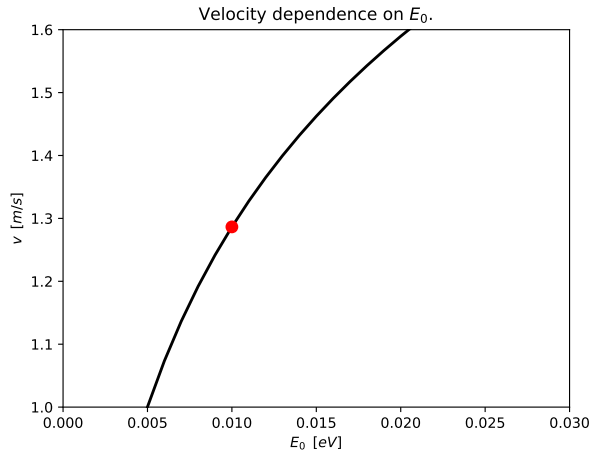


FIG. 5: Velocity dependence on the deposited energy based on Eq. (5). The behavior is as expected: the greater the energy deposited, the higher the velocity. The red dot shows the expected velocity for an energy deposition around 10^{-2} eV. This plot is calculated for a Zeeman energy of 10^{-4} eV for an anisotropic energy barrier of $U = 100$ K. The velocity also depends on how much Zeeman energy is stored, which means that the general behavior will change by changing the temperature at which the sample is kept.

each of the $E_S = \pm S$ sublevels having a particular orientation along the axial anisotropy axis; thus, $E_S = +S$ corresponds to spin up, whereas $E_S = -S$ corresponds to spin down. A pictorial view of the splitting with and without an applied external magnetic field can be found in FIG.4.

In FIG.4a, we plot the crossover between the energy levels and a double well, including a barrier of size U , indicating on the left the negative E_S levels and on the right side, the positive E_S , just to illustrate the degeneracy of the eigenstates, without an applied external magnetic field. In FIG.4b, we exhibit the potential in the presence of an external magnetic field, showing a metastable vacuum state with energy equal to $2\mu_B g J B$ with respect to the true vacuum, where μ_B is the Bohr magnetic moment, g is the gyromagnetic factor, J the total angular momentum and B the magnitude of the applied magnetic field.

These nanomagnets can go from one state to another via various relaxation mechanisms [35, 38, 39]. The most common relaxation processes operating in SMMs are the ones that occur through spin-phonon coupling (phonon being the quantum of the vibration mode of the molecules), namely Orbach, Raman and direct processes. Also, we have those that occur due to the quantum nature of the materials, generally quantum tunnelling of the magnetization and thermally assisted relaxation processes [39]. For our case, we are working with

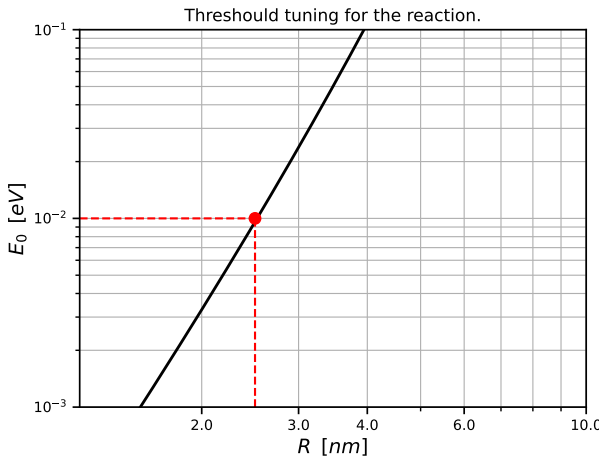


FIG. 6: Tuning of the necessary deposited energy to trigger the reaction. As can be seen for a radius of $R \approx 3\text{nm}$, which is around the value for a SMM of Dy^{III} , the energy deposition is of at least 10^{-2}eV as shown by the red dot and lines.

lanthanides, f-block metals [35] in which the important mechanisms are Orbach and Raman [40]. These involve two-phonon-assisted processes, while the others can involve a single or two phonons. For the Orbach relaxation process, the system overcomes the entire barrier U (See FIG.4b) by absorbing phonons from the crystal lattice containing the exact energy $\hbar\omega_i$ to jump from one of the ground sublevels ($E_S = \pm S$) to the highest excited sublevel ($E_S = 0$), with ω_i being the frequency of the incoming phonons, and so, from this excited state, the system will relax to either the state with $E_S = -S$ or the state with $E_S = +S$ emitting new phonons with energy $\hbar\omega_e$, ω_e being the frequency of the emitted phonon. Therefore, the energy difference between the absorbed and emitted phonon will correspond to the energy difference between the $\pm E_S$ sublevels in the ground state. The Orbach process does not occur between the highest excited states. Instead, this process usually occurs between the first or second excited states. So, a large phonon energy is required for this process to occur, and it usually operates at the highest temperatures. However, for the Raman, the assisted process is driven by the inelastic dispersion of phonons. In this process, the molecule will absorb a phonon with energy $\hbar\omega_i$, reach a virtual excited state, and emit another phonon with energy $\hbar\omega_e$. In that way, the energy difference between the two phonons will correspond to the energy difference between the $\pm E_S$ sublevels in the ground state.

In fact, all these assisted processes happen due to spin-phonon interactions that require energy in the form of thermally assisted energy. For example, a recent study shows, through ab-initio calculation for a Dy^{III} based molecule [40], that the two relaxation processes that

dominate are: Orbach and Raman for high and low temperatures, respectively. As we are interested in the absorption mechanism that injects sufficiently large energies, we use the Orbach relaxation description (for a review, see [35]),

$$\tau_R \approx \tau_0 \exp \left(\frac{U - \frac{1}{2}\Delta E_{\text{Zee}}}{\Delta T} \right), \quad (4)$$

in which U is the size of the energy barrier related directly to D and ΔE_{Zee} is the stored Zeeman energy, τ_0 is the attempt time related to each type of SMM [41], and ΔT is the temperature difference.

Since these molecules might be in a metastable state as shown in FIG 4b, if an $O(1)$ fraction of SMMs is kept in this state, which can be achieved if the system is kept at sufficiently low temperatures ($\sim 1\text{ K}$), we can use them as a mean of directly detecting dark matter. The relaxation of them from the metastable state and thus the release of the stored Zeeman energy in the form of thermal energy induces the relaxation of neighbor molecules and so on, as shown in FIG.1 which sketches the deflagration mechanism, that is known as magnetic avalanche. This process is known and reported and is at the heart of the system's use as a detector and can be measured using micron-sized Hall sensors [28, 42].

Magnetic avalanche is a process in which the rapid release of magnetic energy occurs along a given neighbourhood, in a similar way to a cascade. This process usually occurs in solar flares [43], molecular magnetic materials[42] and in some types of diodes [44]. For molecular crystals, it is possible to demonstrate this phenomenon through local measurements with temporal resolution of the rapid magnetization reversal in millimeter-sized single crystals of Mn_{12} acetate [42]. In this case, the magnetic avalanche takes the form of a thin interface between regions of opposite magnetization. This interface propagates throughout the crystal at a constant speed for a fixed applied field. In fact, the propagation of this interface alters the local magnetization of the molecule within the crystal (see FIG.1) in a similar way to a cascade. Another way to understand this phenomenon is that it is quite analogous to the propagation of a flame front (deflagration) through a flammable chemical substance.

The velocity of magnetic avalanches can be given by a crude estimate using the heat equation [42] for a sample of Mn_{12} -acetate, and can be used to assess the sensitivity of the reaction to that of the deposited energy. The velocity can be determined using Hall sensors that measure the magnetic field in a direction perpendicular to the applied field. Our proposal relies on a different sample, but the same relaxation process drives the deflagration mechanism once DM hits the detector, that is the Orbach routine [40, 42]. Hence, we can use this velocity to assess

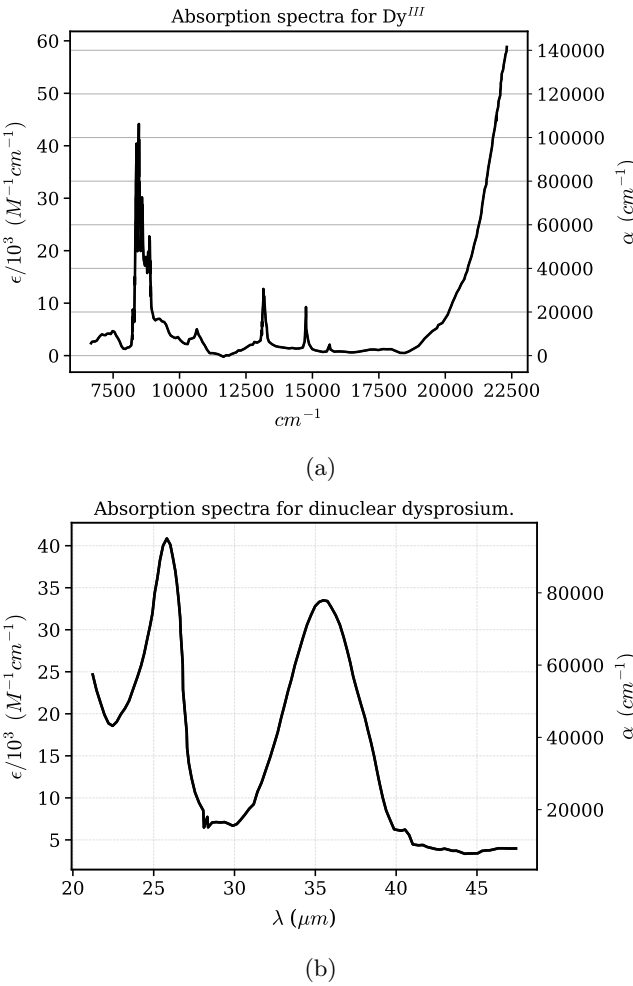


FIG. 7: Absorption spectra of both molecules are considered in the analysis. FIG.7a is the solid-state absorption spectra of UV-vis-NIR for the crystal **1-(P)** as reported from [24]. The x-axis is the wavenumber in cm^{-1} and the y-axis is the absorptivity in cm^{-1} . FIG.7b is the absorption spectra of UV-vis light as reported from [25]. This is the curve that corresponds to complex $\text{Dy}_2(\text{dbm})_4(\text{OQ})_2(\text{CH}_3\text{OH})_2$ synthesized by 8-hydroxyquinoline and dibenzoylmethanate (dbm) ligands. The x-axis corresponds to the wavelength of light, and the left y-axis corresponds to the molecular absorption coefficient and the right y-axis to the absorption coefficient that directly relates to the cross-section via Eq. (10).

the deposited energy of the DM particle,

$$v \sim \sqrt{\frac{\kappa}{\tau_0}} \exp\left(-\frac{U - \frac{1}{2}\Delta E_{\text{Zee}}}{\Delta T}\right), \quad (5)$$

where κ is the thermal diffusivity of the SMMs. This magnetic avalanche propagates as the narrow interface through the crystal at a constant velocity [28, 42]. The temperature difference can be put in terms of the de-

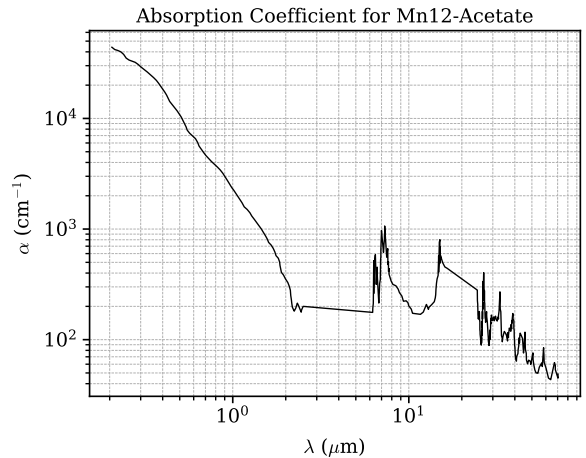


FIG. 8: Absorption coefficient for the Mn12-Acetate, which were taken from [26, 27], considered in the calculation of the kinetic mixing of [23] and on the axion-photon coupling of our work. The flat region in the wavelength interval of $10^0 < \lambda < 10^1$ is an interpolation due to the lack of data.

posited energy E_0 from the DM particle (see Sec.), which can serve as a probe for the signal; this feature can be seen in FIG.5.

SETTING UP THE DETECTOR

In order to find the necessary energy to trigger the magnetic avalanche reaction in a SMM detector, we can follow [23] in comparing the characteristic time of relaxation, τ_R for an Arrhenius law ($\tau_R \approx \tau_0 \exp\left\{\left(\frac{U - \frac{1}{2}\Delta E_{\text{Zee}}}{\Delta T}\right)\right\}$, where τ_0 is a constant related to each SMM and it may vary from $10^{-12} - 10^{-9}$, $\Delta E_{\text{Zee}} = 2\mu_B g_J J B$ is the Zeeman splitting, U the size of the energy barrier and ΔT the difference in temperature) with the time heat takes to dissipate in the detector, τ_D ; considering that we need the SMM to flip before heat dissipates, we need $\tau_R < \tau_D$. With this imposition, we can sense the minimum energy needed if we assume that the SMM will have a Debye behavior for its temperature dependence, which is the observed behavior for SMMs at low temperatures [45]. This approximation yields the following,

$$E_0 \gtrsim \frac{c_0 R^3 (U - \frac{1}{2}\Delta E_{\text{Zee}})^4}{\ln\left(\frac{R^2}{\tau_0 \kappa}\right)}, \quad (6)$$

where c_0 and R are the SMM's volume-specific heat capacity and radius.

Eq. (6) places a lower bound on the energy threshold as a function of R for SMMs. Using the data reported in [25] for the dinuclear Dysprosium illustrated in FIG.2 that

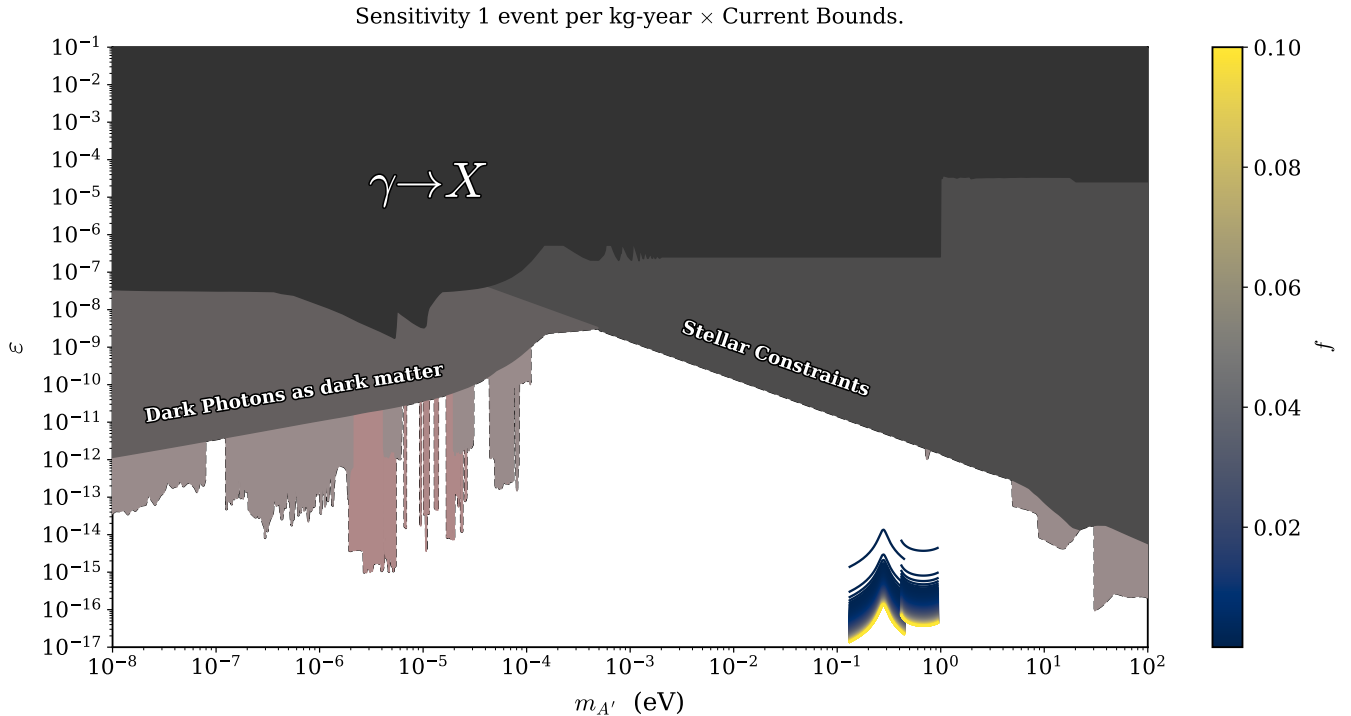


FIG. 9: Expected sensitivity to the kinetic mixing, ε , which governs the interaction with SM fermions. We varied $f = 0.01 - 0.1$. Clearly, dysprosium can be a promising laboratory for *dark photons* with the potential to cover a few orders of unexplored parameter space.

features $\tau \sim 4 \times 10^{-9}$ s, $U = 109.5$ K and $\kappa \sim 10^{-7}$ m²/s at 1K [23], while for Dy^{III} [24] does not report the value of τ_0 , we adopted the same value.

The results are shown in FIG.6, where we can see that for an SMM molecule of radius $\sim (2-3)$ nm, the threshold energy to trigger the reaction will be $\sim 10^{-2}$ eV. Given that the DM velocity in our galaxy is of order $v \sim 10^{-3}$, the average deposited energy is approximately $\sim 10^{-7} - 10^{-6}$ eV, which is insufficient to trigger the reaction. To account for this, we consider that only a fraction f of DM particles will have sufficient energy to initiate the reaction. These particles may originate from a class of physical processes that impart additional energy to DM, a scenario known as Boosted Dark Matter (BDM) [15–18, 46, 47].

RESULTS

In this section, we demonstrate the new physics reach of this proposed detection method for the *dark photon* and *axion* models. In particular, we will assess the sensitivity to the kinetic mixing parameter ε for the *dark photon* dark matter (DPDM), A'_μ , and the *axion*-photon coupling, $g_{a\gamma\gamma}$, for *axion* model. Starting with the *dark photon* model, it is well-known that the kinetic mixing term between the photon and the dark photon in Eq.

(1) induces an interaction between with SM fermions described as follows,

$$\mathcal{L}_{DP} \supset e\varepsilon A'_\mu J^\mu, \quad (7)$$

which is very similar to QED, but with the electric charge suppressed by the kinetic mixing angle ε . Consequently, the interaction cross-section of SM fermions and the dark sector gauge boson can be expressed as the QED cross-section rescaled by ε^2 [29],

$$\sigma_{A'} = \varepsilon^2 \sigma^\gamma. \quad (8)$$

We can reinterpret the average absorption cross section for the *dark photon* model [23, 48],

$$\langle n\sigma_{\text{abs}}(m_{A'})v \rangle \approx \varepsilon^2 \langle n\sigma_{\text{abs}}^\gamma(c=1) \rangle. \quad (9)$$

This approximation arises because the mixing angle for absorption is rescaled by the relative permittivity of the SMM, which can be approximated as unity [23]. This approximation, alongside the rescaling of the *dark photon* cross-section, is helpful because the actual cross-section for photons being absorbed in materials is known [23],

$$\sigma_{\text{abs}}^\gamma = \frac{\alpha}{n}, \quad (10)$$

where α is the absorption coefficient of the material and n its number density. While for the *axion*, its coupling

to the photon is via a dimension five operator in Eq.(2), which leads to [34],

$$\mathcal{L}_a = g_{a\gamma\gamma} a \vec{E} \cdot \vec{B}, \quad (11)$$

where $g_{a\gamma\gamma}$ has dimension of Energy^{-1} . We can determine the total rate of absorption of an *axion* in a magnetized medium per unit exposure,

$$R \simeq \left(\frac{g_{a\gamma\gamma} B_0}{m_a} \right) \frac{\rho_{\text{DM}}}{\rho_{\text{T}}} \text{Im} \left[-\frac{1}{\kappa(m_a)} \right], \quad (12)$$

where m_a is the *axion*'s mass, ρ_{DM} and ρ_{T} are the DM local density, and the target's density, B_0 is the applied magnetic field in the medium, and $\kappa(m_a)$ is the dielectric function evaluated at the *axion*'s mass [33, 49–51] and,

$$g_{a\gamma\gamma} \sim \frac{\varepsilon m_a}{B_0}. \quad (13)$$

Via Eq. (13), we translate the expected sensitivity to the *axion*-photon coupling. Eq. (13) also shows that the *axion*-photon coupling is amenable to the strength of the applied magnetic field, contrary to the kinetic mixing sensitivity, which has no dependence at all in our case. This is a considerable feature for the *axion*, because we can improve the sensitivity through strong magnetic fields, while reducing the energy threshold in Eq. (6). Thus, if we lower the threshold enough, we might not need to work in the framework of Boosted Dark Matter anymore. Nonetheless, to be consistent with the *dark photon* case, we will consider both with the same value of applied magnetic field: $B = 1\text{T}$. Therefore, there is still a need for the BDM framework as Eq. (6) is model independent.

We need to derive the absorption coefficient, α , for the molecules in question to obtain the absorption rate. To do so, we need to use absorbance or transmittance via Beer-Lambert's law,

$$A = -\log_{10} e^{-\alpha h}, \quad (14)$$

where h is the concentration and l the thickness of the material under analysis. To obtain data for the molecules considered, we used [24, 25]. However, the reported data is in terms of the molecular absorption coefficient as can be seen in the left y-axis of FIG. 7, which relates to Beer-Lambert's law in a different form,

$$A = \epsilon \times c \times l, \quad (15)$$

where ϵ is the molecular absorption coefficient, c is the concentration given in $\text{mol/L} = M$, which makes $[\epsilon] = \text{cm}^{-1}\text{M}^{-1}$. The conversion from one to the other is made considering that the molar concentration can be related to the concentration in Eq. (14) by $c = \frac{\rho \times h}{m} \times \frac{10^3}{N_A}$, for ρ , m , and N_A are the density, mass and Avogadro's number of the molecule. Using the molar mass of the

substance in consideration, $\mathcal{M} = \frac{m}{N_A}$, we get the exact relationship between both coefficients,

$$\alpha = 10^3 \ln 10 \frac{\rho}{\mathcal{M}} \epsilon. \quad (16)$$

Using this equation and the data reported in [24, 25] for the density and molecular mass of the substances, we get the exact values for α as a function of wavenumber. The values are shown in the y-axis of FIG.7, where the shape for ϵ and α are the same, because the conversion is independent of the wavelength under consideration. With the exact values for α we can then directly connect the reported data with the prospects for the sensitivity of a DPDM particle being absorbed in the detector.

The reach is found using the rate of interaction of a DM particle in a detector [1],

$$R = \frac{\rho_{\text{DM}}}{m_{\text{DM}}} \frac{1}{\rho} \langle n \sigma v \rangle, \quad (17)$$

where ρ_{DM} and m_{DM} are the density and the mass of DM respectively, ρ and n are the density and number density of the crystal and v is the DM velocity, which can be regarded as $v \approx 10^{-3}$, however when we substitute Eq. (9) in Eq. (17) there will be no velocity dependence, therefore when working in the framework of BDM to account for the triggering the reaction as explained in Sec. (6), we only need to add on Eq. (17) a new term f that account for the fraction of DM in our Solar System that is boosted and reaches the detector, Eq. (17) becomes,

$$R \simeq f \frac{\rho_{\text{DM}}}{m_{\text{DM}}} \frac{1}{\rho} \langle n \sigma_{\text{abs}}^{\gamma} \rangle, \quad (18)$$

where f represents the fraction of BDM. We derive the rate by inserting Eq. (9) in Eq. (18) using absorption data plotted in FIGs. 7a and 7b. The expected sensitivity is then calculated for $\omega = m_{A'}$ for a given DM mass in FIG.11 for $f = 10^{-5} - 10^{-1}$.

The expected sensitivity in FIG.9 declines as the amount of BDM available for absorption in the detector decreases. The cusp in the mass region between $10^{-1} - 10^0$ is related to the data in FIG.7a. As can be seen, the absorption gets close enough to zero at 12000cm^{-1} , and given the kinetic mixing dependence on the absorption coefficient scales as $\propto 1/\alpha^{\frac{1}{2}}$, it is to be expected to behave as presented in the FIG.9. FIG. 9 explicitly shows the expected sensitivity for an exposure of 1 event per kg-year. We put our findings into perspective with current bounds on *dark photons* [52, 53]. In the mass region of interest, the limits neither come directly from direct detection experiments nor from *dark photon* dark matter searches. Nevertheless, the scientific reach of our proposal surpasses that of existing experiments, being able to cover a large region of untouched parameter space.

In particular, the shaded regions are labeled accordingly to the type of experiments in question; $\gamma \rightarrow X$ are

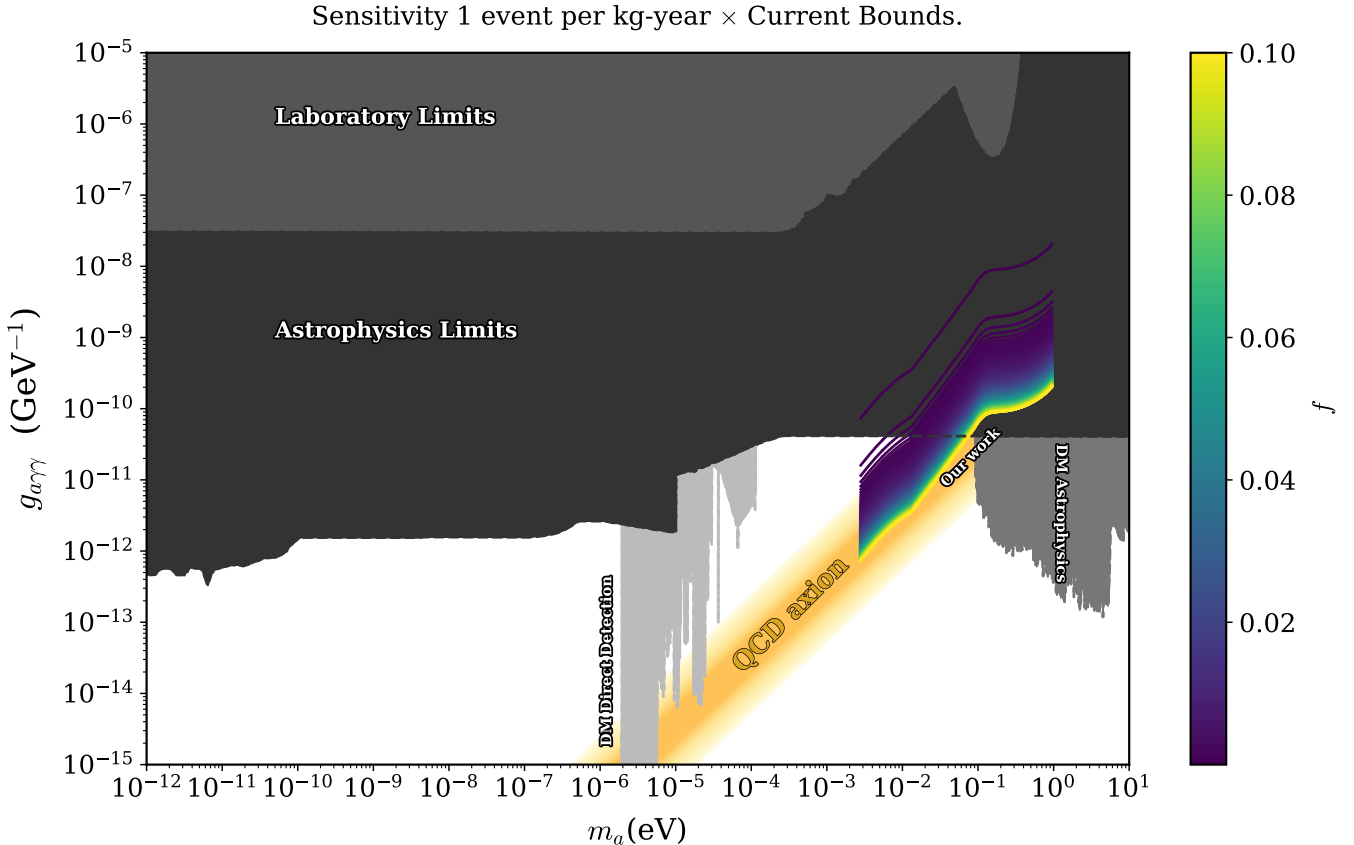


FIG. 10: Expected reach to the *axion*-photon coupling overlaid with existing bounds in gray. For $m_a < 10^{-1}$ eV our proposal yields a promising sensitivity. We have varied the fraction of boosted dark matter in the range $f = 0.01 - 0.1$.

laboratory limits in ε coming from light shining through a wall [54–56], Cavendish-Coulomb [57]; *dark photon* as Dark Matter are the limits for the DP corresponding to the totality of DM [58–61], and Stellar Constraints come from astrophysics limits [62–64]; the other colored regions without labels refer to Direct Detection experiments [3–5, 65] in the mass region of $10^0 - 10^2$, and other laboratory experiments, such as the measurement of Dark-E fields [66] or radio frequency cavity searches [67] for the lower mass region: $10^{-8} - 10^{-4}$. The blue-to-yellow region corresponds to our calculations for the two new proposed molecules: Dy2 [24] and Dy^{III} [25].

As aforementioned, we can reinterpret these results for *axions*. Using the absorption spectra for dinuclear dysprosium and assuming 1 event per kg-year of exposure, we ended up probing a region of parameter space already excluded by *axion* searches (see Appendix). That said, we adopted the Mn12-acetate, a complex compound of manganese, and repeated the entire procedure described above and derived the expected sensitivity to *axions* as displayed in FIG.10 adopting a magnetic field $B_0 = 1$ T.

The shape of the curve is very similar to that of the *dark photon* model. The break exhibited in the curve of

FIG.10 has to do with the linear dependence in the mass that appears for the coupling, which is not present in the case of the *dark photon* model. The projected sensitivity can be improved using a stronger magnetic field.

We have superimposed the existing limits in the literature [53]. These bounds stem from laboratory searches [68–71], astrophysics searches for *axions* not as DM [72–83], astrophysics bounds for *axions* as DM [84–91], and DM direct detection bounds [92–94].

The purple-to-yellow colored region is a result of our estimate based on Eq. (13). The expected reach becomes promising masses $m_a < 10^{-1}$ eV. We emphasize that we can increase the applied magnetic field to improve the sensitivity. From FIG.10, it is clear that our proposal offers the possibility to probe a sizable region of the QCD *axion* parameter space, with leading sensitivity for *axion* masses between 2×10^{-3} and 8×10^{-2} eV. It is worth noticing that we can push down these projections if we either increase the applied magnetic field or consider a higher fraction of BDM than the one considered in the plots.

In summary, by integrating concepts from particle physics, condensed-matter physics, and chemistry, we

demonstrate that interdisciplinary approaches can enable genuinely new detection strategies and open access to previously unexplored regions of parameter space.

CONCLUSION

The community has been dedicated to testing the compelling WIMP paradigm via accelerators, direct and indirect detection experiments, but null results have been reported thus far. This has motivated the community to explore other dark matter candidates and novel detection mechanisms. In this spirit, we propose to use Single Molecule Magnets as dark matter laboratories, particularly focused on the *dark photon* and *axion* models.

Single Molecule Magnets function as frustrated systems stabilized in metastable states for relatively long periods. Dark-matter absorption triggers accelerated relaxation from these states, producing detectable magnetic avalanches. Using dysprosium- and manganese-based molecules, we computed reaction rates for dark-photon and axion interactions, deriving projected sensitivities. Our analysis demonstrates that dysprosium SMMs improve sensitivity to dark photons by orders of magnitude, while manganese systems probe previously inaccessible regions of the QCD axion parameter space.

Our work builds a bridge between chemistry, condensed-matter physics, and particle physics for dark-matter detection. Future characterization of magnetic materials across infrared to ultraviolet frequencies will critically enhance the sensitivity of this approach and pave the road for the potential detection of dark matter particles.

ACKNOWLEDGMENTS

The authors thank Raimundo Silva and Jacinto P. Neto for insightful discussions. FSQ thanks CERN and the Max Planck Institute for Nuclear Physics for the hospitality where this work was partly developed. JA is funded by the *Coordenação de Aperfeiçoamento de Pessoal de Nível Superior (CAPES)* and CNPq grants 88887.989987/2024-00 and 403521/2024-6. FSQ acknowledges support from Simons Foundation (Award Number:1023171-RC), CNPq 403521/2024-6, 408295/2021-0, 403521/2024-6, 406919/2025-9, 351851/2025-9, the FAPESP Grants 2021/01089-1, 2023/01197-4, ICTP-SAIFR 2021/14335-0, and the ANID-Millennium Science Initiative Program ICN2019_044. This work is partially funded by FINEP under project 213/2024 and was carried out in part through the IIP cluster *bulletcluster*.

APPENDIX A

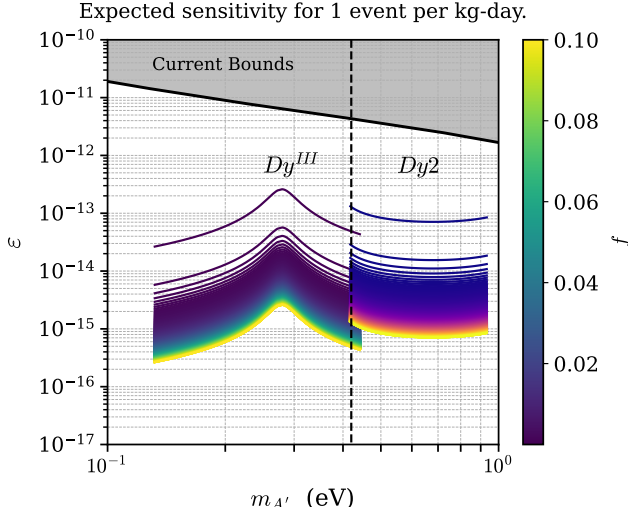
In this section, we present the sensitivity with an exposure of 1 event per kg-day to both *dark photon* and *axion* dark matter particles. These plots are an extension of the results are exhibited in FIGs.9-10 but offer a clearer vision of the scientific reach in comparison with existing bounds and the role of each compound.

In FIGs.11a-11b we display the sensitivity for two different exposures using dysprosium molecules. Notoriously, with a larger exposure, a greater reach is obtained. This behavior is expected since the kinetic mixing scales as $(\text{kg-time})^{-1/2}$. These findings were derived using Eq. (18) for $f = 0.01 - 0.1$. From FIGs.11a-11b, we solidly show that such molecules offer a powerful platform for probing physics beyond the Standard Model.

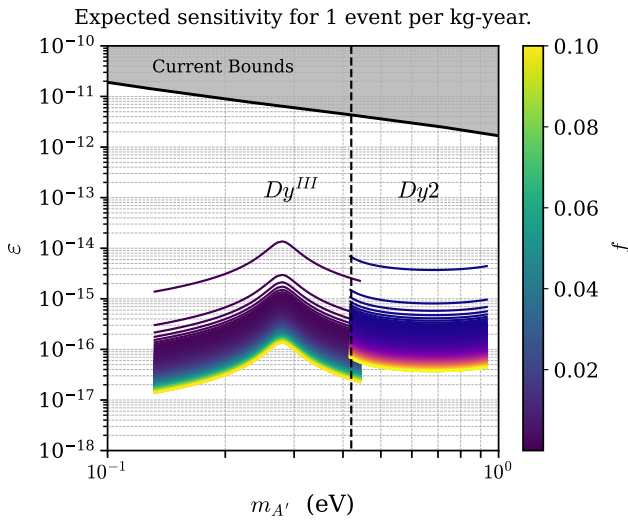
Using the same molecules, we also derived the sensitivity to the *axion*-photon coupling. The results are summarized in FIG.12 for an exposure of 1 event per kg-year. The parameter space covered in FIG.12 has already been excluded. Thus, we decided to use a different molecule, Mn12-acetate, which is a complex compound of manganese, and repeat the same procedure. The expected reach is shown in FIGs.13a-13b for different exposures, similar to the previous figures. Our finding is based on Eq. (13) and the sensitivity projected for kinetic mixing using Mn12-acetate [23]. The shape of the curve is very similar to that of the *dark photon* model. The small tilt in FIGs.13a-13b is due to the linear dependence in the mass that appears for the coupling, which is not present in the case of the kinetic mixing. We have adopted a magnetic field $B_0 = 1\text{T}$, but a better sensitivity can be achieved with larger magnetic fields.

Our findings were based on two compounds, and for this reason, there is a visible break in the curves. In particular, we observe that dy2 covers larger masses compared to the Dy^{III} .

- [1] Cirelli, M., Strumia, A. & Zupan, J. *Dark Matter* (2024). 2406.01705.
- [2] Green, A. M. Primordial black holes as a dark matter candidate - a brief overview. *Nucl. Phys. B* **1003**, 116494 (2024). 2402.15211.
- [3] Schumann, M. Direct Detection of WIMP Dark Matter: Concepts and Status. *J. Phys. G* **46**, 103003 (2019). 1903.03026.
- [4] Aprile, E. *et al.* First Dark Matter Search with Nuclear Recoils from the XENONnT Experiment. *Phys. Rev. Lett.* **131**, 041003 (2023). 2303.14729.
- [5] Aprile, E. *et al.* Search for Light Dark Matter in Low-Energy Ionization Signals from XENONnT. *Phys. Rev. Lett.* **134**, 161004 (2025). 2411.15289.
- [6] Gaskins, J. M. A review of indirect searches for particle dark matter. *Contemp. Phys.* **57**, 496–525 (2016). 1604.00014.



(a) Sensitivity for the kinetic mixing with an exposure of 1 event per kg-day.



(b) Sensitivity for the kinetic mixing with one event per kg-year exposure.

FIG. 11: Expected sensitivities for different exposure times for the *dark photon* model assuming: (a) 1 event per kg-day; (b) one event per kg-year.

- [7] Albert, A. *et al.* Searching for Dark Matter Annihilation in Recently Discovered Milky Way Satellites with Fermi-LAT. *Astrophys. J.* **834**, 110 (2017). 1611.03184.
- [8] Boveia, A. & Doglioni, C. Dark Matter Searches at Colliders. *Ann. Rev. Nucl. Part. Sci.* **68**, 429–459 (2018). 1810.12238.
- [9] Perez Adan, D. Dark Matter searches at CMS and ATLAS. In *56th Rencontres de Moriond on Electroweak Interactions and Unified Theories* (2023). 2301.10141.
- [10] Wang, J.-W. Blazar-boosted dark matter: Novel signatures via elastic and inelastic scattering. *Phys. Rev. D* **112**, 055004 (2025). 2503.22105.
- [11] Essig, R., Manalaysay, A., Mardon, J., Sorensen, P. &

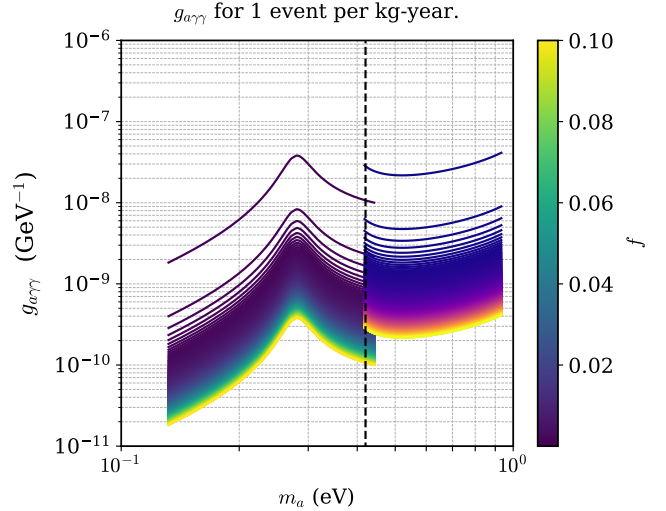


FIG. 12: Expected reach to *axion-photon* coupling for the dysprosium molecules assuming 1 event per kg-year.

- Volansky, T. First Direct Detection Limits on sub-GeV Dark Matter from XENON10. *Phys. Rev. Lett.* **109**, 021301 (2012). 1206.2644.
- [12] Essig, R., Volansky, T. & Yu, T.-T. New Constraints and Prospects for sub-GeV Dark Matter Scattering off Electrons in Xenon. *Phys. Rev. D* **96**, 043017 (2017). 1703.00910.
- [13] Ghosh, D. K., Gupta, T., Heikinheimo, M., Huitu, K. & Jeesun, S. Boosted dark matter driven by cosmic rays and diffuse supernova neutrinos. *Phys. Rev. D* **111**, 063019 (2025). 2411.11973.
- [14] Agashe, K., Cui, Y., Necib, L. & Thaler, J. (In)direct Detection of Boosted Dark Matter. *JCAP* **10**, 062 (2014). 1405.7370.
- [15] Bringmann, T. & Pospelov, M. Novel direct detection constraints on light dark matter. *Phys. Rev. Lett.* **122**, 171801 (2019). 1810.10543.
- [16] Das, A., Herbermann, T., Sen, M. & Takhistov, V. Energy-dependent boosted DM from DSNB. *PoS* **NOW2024**, 014 (2025).
- [17] Herbermann, T., Lindner, M. & Sen, M. Attenuation of cosmic ray electron boosted dark matter. *Phys. Rev. D* **110**, 123023 (2024). 2408.02721.
- [18] Das, A., Herbermann, T., Sen, M. & Takhistov, V. Energy-dependent boosted dark matter from diffuse supernova neutrino background. *JCAP* **07**, 045 (2024). 2403.15367.
- [19] Hochberg, Y., Lin, T. & Zurek, K. M. Absorption of light dark matter in semiconductors. *Phys. Rev. D* **95**, 023013 (2017). 1608.01994.
- [20] Kahn, Y. & Lin, T. Searches for light dark matter using condensed matter systems. *Rept. Prog. Phys.* **85**, 066901 (2022). 2108.03239.
- [21] Herrera, F. & Spano, F. C. Dark Vibronic Polaritons and the Spectroscopy of Organic Microcavities. *Phys. Rev. Lett.* **118**, 223601 (2017). 1610.04252.
- [22] Hochberg, Y., Pyle, M., Zhao, Y. & Zurek, K. M. Detecting Superlight Dark Matter with Fermi-Degenerate Materials. *JHEP* **08**, 057 (2016). 1512.04533.

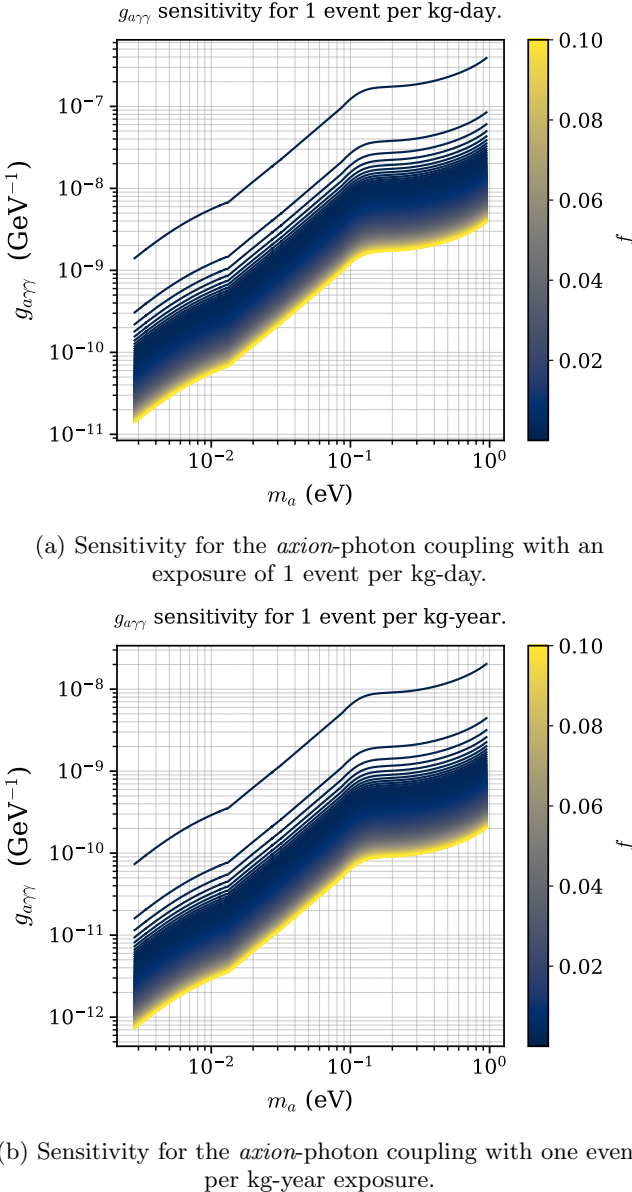


FIG. 13: Projected reach of a manganese compound to the *axion-photon* coupling using 1 one event per kg-day (figure a), and 1 one event per kg-day (figure b).

- [23] Bunting, P. C., Gratta, G., Melia, T. & Rajendran, S. Magnetic bubble chambers and sub-gev dark matter direct detection. *Physical Review D* **95** (2017). URL <http://dx.doi.org/10.1103/PhysRevD.95.095001>.
- [24] Raju, M. S. *et al.* Magneto-chiral dichroism in a one-dimensional assembly of helical dysprosium(iii) single-molecule magnets. *Inorganic Chemistry* **62**, 17583–17587 (2023). URL <https://doi.org/10.1021/acs.inorgchem.3c03204>.
- [25] Shen, H.-Y., Wang, W.-M., Gao, H.-L. & Cui, J.-Z. Near-infrared luminescence and smm behaviors of a family of dinuclear lanthanide 8-quinolinolate complexes. *RSC Advances* **6**, 34165–34174 (2016). URL <https://doi.org/10.1039/C6RA02656G>.

- [26] Sushkov, A. B. *et al.* Magnetic field effects on the far-infrared absorption in mn₁₂-acetate. *Phys. Rev. B* **63**, 214408 (2001). URL <https://link.aps.org/doi/10.1103/PhysRevB.63.214408>.
- [27] Oppenheimer, S. M., Sushkov, A. B., Musfeldt, J. L., Achey, R. M. & Dalal, N. S. Diffuse optical excitations in mn₁₂-acetate. *Phys. Rev. B* **65**, 054419 (2002). URL <https://link.aps.org/doi/10.1103/PhysRevB.65.054419>.
- [28] Friedman, J. R. & Sarachik, M. P. Single-molecule nanomagnets. *Annual Review of Condensed Matter Physics* **1**, 109–128 (2010). URL <http://dx.doi.org/10.1146/annurev-conmatphys-070909-104053>.
- [29] Fabbrichesi, M., Gabrielli, E. & Lanfranchi, G. *The Physics of the Dark Photon: A Primer* (Springer International Publishing, 2021). URL <http://dx.doi.org/10.1007/978-3-030-62519-1>.
- [30] Peccei, R. D. & Quinn, H. R. CP Conservation in the Presence of Instantons. *Phys. Rev. Lett.* **38**, 1440–1443 (1977).
- [31] Preskill, J., Wise, M. B. & Wilczek, F. Cosmology of the Invisible Axion. *Phys. Lett. B* **120**, 127–132 (1983).
- [32] Kim, J. E. & Carosi, G. Axions and the Strong CP Problem. *Rev. Mod. Phys.* **82**, 557–602 (2010). [Erratum: Rev.Mod.Phys. 91, 049902 (2019)], 0807.3125.
- [33] Berlin, A. & Trickl, T. Absorption of Axion Dark Matter in a Magnetized Medium. *Phys. Rev. Lett.* **132**, 181801 (2024). 2305.05681.
- [34] Navas, S. *et al.* Review of particle physics. *Phys. Rev. D* **110**, 030001 (2024).
- [35] Zabala-Lekuona, A., Seco, J. M. & Colacio, E. Single-molecule magnets: From mn₁₂-ac to dysprosium metallocenes, a travel in time. *Coordination Chemistry Reviews* **441**, 213984 (2021). URL <https://www.sciencedirect.com/science/article/pii/S0010854521002587>.
- [36] Orts-Arroyo, M., Rojas, C., Moliner, N. & Martínez-Lillo, J. Lipoic acid-functionalized hexanuclear manganese(iii) nanomagnets suitable for surface grafting. *International Journal of Molecular Sciences* **24**, 8645 (2023).
- [37] Sessoli, R., Gatteschi, D., Caneschi, A. & Novak, M. Magnetic bistability in a metal-ion cluster. *Nature* **365**, 141–143 (1993).
- [38] Moreno-Pineda, E., Taran, G., Wernsdorfer, W. & Ruben, M. Quantum tunnelling of the magnetisation in single-molecule magnet isotopologue dimers. *Chem. Sci.* **10**, 5138–5145 (2019). URL <http://dx.doi.org/10.1039/C9SC01062A>.
- [39] Abragam, A. & Bleaney, B. *Electron Paramagnetic Resonance of Transition Ions*. Oxford Classic Texts in the Physical Sciences (Oxford, 2012). URL <https://books.google.com.br/books?id=ASNoAgAAQBAJ>.
- [40] Briganti, M. *et al.* A complete ab initio view of orbach and raman spin-lattice relaxation in a dysprosium coordination compound. *J. Am. Chem. Soc.* **143**, 13633–13645 (2021). URL <https://doi.org/10.1021/jacs.1c05068>.
- [41] Suzuki, Y. *et al.* Propagation of avalanches in mn₁₂-acetate: Magnetic deflagration. *Phys. Rev. Lett.* **95**, 147201 (2005). URL <https://link.aps.org/doi/10.1103/PhysRevLett.95.147201>.
- [42] Suzuki, Y. *et al.* Propagation of avalanches in mn₁₂-acetate: Magnetic deflagration. *Phys. Rev. Lett.* **95**,

147201 (2005). URL <https://link.aps.org/doi/10.1103/PhysRevLett.95.147201>.

[43] Charbonneau, P., McIntosh, S. W., Liu, H.-L. & Bogdan, T. J. Avalanche models for solar flares (Invited Review). *Solphys* **203**, 321–353 (2001).

[44] McLuckie, I. F. Investigation of zener and avalanche diode characteristics. *Physics Education* **23**, 251 (1988). URL <https://doi.org/10.1088/0031-9120/23/4/417>.

[45] Miyazaki, Y. *et al.* Magnetic-field-dependent heat capacity of the single-molecule magnet [Mn₁₂O₁₂(O₂C₆H₄O)₁₆(H₂O)₃]. *Inorganic Chemistry* **40**, 6632–6636 (2001). URL <https://doi.org/10.1021/ic010567w>.

[46] Abe, K. *et al.* Search for Cosmic-Ray Boosted Sub-GeV Dark Matter Using Recoil Protons at Super-Kamiokande. *Phys. Rev. Lett.* **130**, 031802 (2023). [Erratum: *Phys. Rev. Lett.* 131, 159903 (2023)], 2209.14968.

[47] Granelli, A., Ullio, P. & Wang, J.-W. Blazar-boosted dark matter at Super-Kamiokande. *JCAP* **07**, 013 (2022). 2202.07598.

[48] An, H., Pospelov, M., Pradler, J. & Ritz, A. Direct detection constraints on dark photon dark matter. *Physics Letters B* **747**, 331–338 (2015). URL <http://dx.doi.org/10.1016/j.physletb.2015.06.018>.

[49] Hochberg, Y., Pyle, M., Zhao, Y. & Zurek, K. M. Detecting superlight dark matter with fermi-degenerate materials. *Journal of High Energy Physics* **2016** (2016). URL [http://dx.doi.org/10.1007/JHEP08\(2016\)057](http://dx.doi.org/10.1007/JHEP08(2016)057).

[50] Mitridate, A., Trickle, T., Zhang, Z. & Zurek, K. M. Dark matter absorption via electronic excitations. *JHEP* **09**, 123 (2021). 2106.12586.

[51] Catena, R. *et al.* Dark matter-electron interactions in materials beyond the dark photon model. *JCAP* **03**, 052 (2023). 2210.07305.

[52] Caputo, A., Millar, A. J., O’Hare, C. A. & Vitagliano, E. Dark photon limits: A handbook. *Physical Review D* **104** (2021). URL <http://dx.doi.org/10.1103/PhysRevD.104.095029>.

[53] O’Hare, C. cajohare/axionlimits: Axionlimits. <https://cajohare.github.io/AxionLimits/> (2020).

[54] Parker, S. R., Hartnett, J. G., Povey, R. G. & Tobar, M. E. Cryogenic resonant microwave cavity searches for hidden sector photons. *Phys. Rev. D* **88**, 112004 (2013). 1410.5244.

[55] Povey, R., Hartnett, J. & Tobar, M. Microwave cavity light shining through a wall optimization and experiment. *Phys. Rev. D* **82**, 052003 (2010). 1003.0964.

[56] Inada, T. *et al.* Results of a Search for Paraphotons with Intense X-ray Beams at SPring-8. *Phys. Lett. B* **722**, 301–304 (2013). 1301.6557.

[57] Kroff, D. & Malta, P. C. Constraining hidden photons via atomic force microscope measurements and the Plimpton-Lawton experiment. *Phys. Rev. D* **102**, 095015 (2020). 2008.02209.

[58] Arias, P. *et al.* WISPy Cold Dark Matter. *JCAP* **06**, 013 (2012). 1201.5902.

[59] McDermott, S. D. & Witte, S. J. Cosmological evolution of light dark photon dark matter. *Phys. Rev. D* **101**, 063030 (2020). 1911.05086.

[60] Witte, S. J., Rosauro-Alcaraz, S., McDermott, S. D. & Poulin, V. Dark photon dark matter in the presence of inhomogeneous structure. *JHEP* **06**, 132 (2020). 2003.13698.

[61] Caputo, A., Liu, H., Mishra-Sharma, S. & Ruderman, J. T. Modeling Dark Photon Oscillations in Our Inhomogeneous Universe. *Phys. Rev. D* **102**, 103533 (2020). 2004.06733.

[62] Dubovsky, S. & Hernández-Chifflet, G. Heating up the Galaxy with Hidden Photons. *JCAP* **12**, 054 (2015). 1509.00039.

[63] Wadekar, D. & Farrar, G. R. Gas-rich dwarf galaxies as a new probe of dark matter interactions with ordinary matter. *Phys. Rev. D* **103**, 123028 (2021). 1903.12190.

[64] Bhoonah, A., Bramante, J. & Song, N. Superradiant Searches for Dark Photons in Two Stage Atomic Transitions. *Phys. Rev. D* **101**, 055040 (2020). 1909.07387.

[65] Aralis, T. *et al.* Constraints on dark photons and axion-like particles from the SuperCDMS Soudan experiment. *Phys. Rev. D* **101**, 052008 (2020). [Erratum: *Phys. Rev. D* 103, 039901 (2021)], 1911.11905.

[66] Godfrey, B. *et al.* Search for dark photon dark matter: Dark E field radio pilot experiment. *Phys. Rev. D* **104**, 012013 (2021). 2101.02805.

[67] Nguyen, L. H., Lobanov, A. & Horns, D. First results from the WISPyDMX radio frequency cavity searches for hidden photon dark matter. *JCAP* **10**, 014 (2019). 1907.12449.

[68] Ballou, R. *et al.* New exclusion limits on scalar and pseudoscalar axionlike particles from light shining through a wall. *Phys. Rev. D* **92**, 092002 (2015). 1506.08082.

[69] Ehret, K. *et al.* New ALPS Results on Hidden-Sector Lightweights. *Phys. Lett. B* **689**, 149–155 (2010). 1004.1313.

[70] Betz, M., Caspers, F., Gasior, M., Thumm, M. & Rieger, S. W. First results of the CERN Resonant Weakly Interacting sub-eV Particle Search (CROWS). *Phys. Rev. D* **88**, 075014 (2013). 1310.8098.

[71] Della Valle, F. *et al.* The PVLAS experiment: measuring vacuum magnetic birefringence and dichroism with a birefringent Fabry-Perot cavity. *Eur. Phys. J. C* **76**, 24 (2016). 1510.08052.

[72] Ayala, A., Domínguez, I., Giannotti, M., Mirizzi, A. & Straniero, O. Revisiting the bound on axion-photon coupling from Globular Clusters. *Phys. Rev. Lett.* **113**, 191302 (2014). 1406.6053.

[73] Dolan, M. J., Hiskens, F. J. & Volkas, R. R. Advancing globular cluster constraints on the axion-photon coupling. *JCAP* **10**, 096 (2022). 2207.03102.

[74] Andriamonje, S. *et al.* An Improved limit on the axion-photon coupling from the CAST experiment. *JCAP* **04**, 010 (2007). hep-ex/0702006.

[75] Ajello, M. *et al.* Search for Spectral Irregularities due to Photon-Axionlike-Particle Oscillations with the Fermi Large Area Telescope. *Phys. Rev. Lett.* **116**, 161101 (2016). 1603.06978.

[76] Meyer, M., Giannotti, M., Mirizzi, A., Conrad, J. & Sánchez-Conde, M. A. Fermi Large Area Telescope as a Galactic Supernovae Axionscope. *Phys. Rev. Lett.* **118**, 011103 (2017). 1609.02350.

[77] Meyer, M. & Petrushevska, T. Search for Axionlike-Particle-Induced Prompt γ -Ray Emission from Extragalactic Core-Collapse Supernovae with the Fermi Large Area Telescope. *Phys. Rev. Lett.* **124**, 231101 (2020). [Erratum: *Phys. Rev. Lett.* 125, 119901 (2020)], 2006.06722.

[78] Davies, J., Meyer, M. & Cotter, G. Constraints on axionlike particles from a combined analysis of three flaring Fermi flat-spectrum radio quasars. *Phys. Rev. D* **107**, 083027 (2023). 2211.03414.

[79] Noordhuis, D. *et al.* Novel Constraints on Axions Produced in Pulsar Polar-Cap Cascades. *Phys. Rev. Lett.* **131**, 111004 (2023). 2209.09917.

[80] Dessert, C., Long, A. J. & Safdi, B. R. No Evidence for Axions from Chandra Observation of the Magnetic White Dwarf RE J0317-853. *Phys. Rev. Lett.* **128**, 071102 (2022). 2104.12772.

[81] Dessert, C., Dunsky, D. & Safdi, B. R. Upper limit on the axion-photon coupling from magnetic white dwarf polarization. *Phys. Rev. D* **105**, 103034 (2022). 2203.04319.

[82] Benabou, J. N. *et al.* Search for Axions in Magnetic White Dwarf Polarization at Lick and Keck Observatories (2025). 2504.12377.

[83] Ning, O. & Safdi, B. R. Leading Axion-Photon Sensitivity with NuSTAR Observations of M82 and M87. *Phys. Rev. Lett.* **134**, 171003 (2025). 2404.14476.

[84] Janish, R. & Pinetti, E. Hunting Dark Matter Lines in the Infrared Background with the James Webb Space Telescope. *Phys. Rev. Lett.* **134**, 071002 (2025). 2310.15395.

[85] Pinetti, E. First constraints on QCD axion dark matter using James Webb Space Telescope observations (2025). 2503.11753.

[86] Saha, A. K., Bouri, S., Das, A., Dubey, A. & Laha, R. Shedding Infrared Light on QCD Axion and ALP Dark Matter with JWST (2025). 2503.14582.

[87] Todarello, E. *et al.* Robust bounds on ALP dark matter from dwarf spheroidal galaxies in the optical MUSE-Faint survey. *JCAP* **05**, 043 (2024). 2307.07403.

[88] Wang, H. *et al.* Spectroscopic search for optical emission lines from dark matter decay. *Phys. Rev. D* **110**, 103007 (2024). 2311.05476.

[89] Nakayama, K. & Yin, W. Anisotropic cosmic optical background bound for decaying dark matter in light of the LORRI anomaly. *Phys. Rev. D* **106**, 103505 (2022). 2205.01079.

[90] Carenza, P., Lucente, G. & Vitagliano, E. Probing the blue axion with cosmic optical background anisotropies. *Phys. Rev. D* **107**, 083032 (2023). 2301.06560.

[91] Todarello, E. & Regis, M. Bounds on axions-like particles shining in the ultra-violet. *JCAP* **05**, 070 (2025). 2412.02543.

[92] Carosi, G. *et al.* Search for Axion Dark Matter from 1.1 to 1.3 GHz with ADMX. *Phys. Rev. Lett.* **135**, 191001 (2025). 2504.07279.

[93] Wuensch, W. *et al.* Results of a Laboratory Search for Cosmic Axions and Other Weakly Coupled Light Particles. *Phys. Rev. D* **40**, 3153 (1989).

[94] Bae, S. *et al.* Search for Dark Matter Axions with Tunable TM020 Mode. *Phys. Rev. Lett.* **133**, 211803 (2024). 2403.13390.